Authentication and Quantification of Extra Virgin Olive Oils by Attenuated Total Reflectance Infrared Spectroscopy Using Silver Halide Fiber Probes and Partial Least-Squares Calibration

LUKAS KÜPPER, H. MICHAEL HEISE,* PETER LAMPEN, ANTONY N. DAVIES, and PETER McINTYRE

Institute of Spectrochemistry and Applied Spectroscopy, Bunsen-Kirchhoff-Str. 11, D-44139 Dortmund, Germany (L.K., H.M.H., P.L., A.N.D.); and School of Applied Sciences, University of Glamorgan, Pontypridd, Mid-Glamorgan, CF37 1DL, U.K. (P.M.)

Infrared attenuated total reflectance spectroscopy has been assessed for the analysis of extra virgin olive oil samples from various Mediterranean sites and their adulteration by sunflower oil. In this study two different silver halide fiber-optic probes were separately tested for the mid-infrared spectroscopic measurement of pure olive oil samples and these same oils adulterated with sunflower oil. One fiber-optic probe contained an exchangeable U-shaped section of the silver halide fiber, whereas the second probe consisted of a fiber-coupled diamond crystal, which performed slightly less well than the whole fiber probe. The optimum standard error of prediction for the sunflower oil concentrations in spiked olive oil samples, obtained by optimized partial least-squares (PLS) calibration models and leave-one-out cross-validation, was 1.2% by weight with the use of a special variable selection strategy based on a pairwise consideration of significant respective minima and maxima of the optimum PLS regression vector, calculated for broad spectral intervals. Calibration robustness was proven by also using packages of 10 randomly selected samples within a further cross-validation for calculating independent prediction values. The implications for product monitoring are discussed.

Index Headings: **Infrared spectroscopy; Attenuated total reflection; Silver halide fibers; Fiber-optic probes; Partial least-squares; Food quality analysis; Olive oil adulteration.**

INTRODUCTION

Mid-infrared spectroscopy has been applied in only a few cases to the analysis of food products due to several reasons. Mid-infrared spectra are rather complex, and, in most cases, water is the major constituent of biosamples. However, water-free samples were recently studied by Dolmatova et al. when identifying modified starches.[1] More recently, the development of new analytical tools has been reported, especially within the clinical chemistry field,[2] where the handling of aqueous samples has been mastered successfully.

Mid-infrared spectroscopy, using in particular the attenuated total reflection (ATR) technique, shows enormous potential for the quantitative multicomponent analysis of biofluids. For process analysis, different approaches have been used. One is the use of flow-through cells, for which the Circle cell from Spectra-Tech is a widely used accessory, although other designs have been proposed—e.g., the Tunnel cell from Axiom Analytical, Inc. The optical design of the latter has also been used in immersion probes, employed, for example, for batch reaction vessel monitoring.[3] Another example of the use of the ATR technique has been described by Picque et al.[4] for the analysis of alcohol and lactate within a fermentation process, and the determination of different sugars in sugar cane juices has been illustrated by Cadet et al.[5]

Recently, the availability of mid-infrared fibers extruded from polycrystalline silver halide materials has enabled the construction of low-cost accessories. Aqueous glucose measurements have been accomplished by using fiber-optic evanescent-wave spectroscopy and a tunable CO_2 laser.[6] The low optical losses within the fiber allow the construction of flexible probes, which can, for example, be employed by the analyst for easy remote sample analysis. In a recent study, spectra of *in vivo* skin tissue of healthy subjects and of various cases of melanoma and nevus, measured by just such a technique, were reported.[7] Our previous experiences with fiber-optic probes have also been published.[8,9]

Our interest here is in samples of vegetable oils, which play an important role in avoiding malnutrition. The determination of the authenticity of extra virgin olive oils has become more important in recent years due to the discovery of the deliberate adulteration and contamination of such products. There is significant economic advantage to be gained from marketing lower quality products in the guise of top-quality oils. The assays of such olive oil samples are difficult due to the composition of the natural products, which show a variability through different growing conditions (soils, climatic differences, harvesting time, and plant genus themselves producing fruits with slight differences in composition due to their genetic variance). In the past, a number of alternative techniques for assessing quality and authenticity have been reported which include gas chromatography,[10] CO_2 laser infrared optothermal spectroscopy,[11] and near-infrared spectroscopy.[12]

Early investigations on quantitative assays for adulterants in extra virgin olive oil samples were carried out by Lai et al.,[13] who employed ATR mid-infrared spectroscopy and partial least-squares (PLS) regression. Classification of different vegetable oils was performed by Dupuy et al.,[14] who used, besides a horizontal ATR accessory, a chalcogenide fiber probe from Graseby-Specac. Wavelength selection was necessary for a further classification study to be successful for the identification of various oils,[15] and the importance of specific bands within

Received 24 October 2000; accepted 18 January 2001.
* Author to whom correspondence should be sent.

0003-7028/01/5505-0563$2.00/0

TABLE I. Characteristics of the silver halide optical fiber.

Structure	Uncladded fiber
Core material	Solid solution of AgBr/AgCl/AgI
Core size diameter	750 μm
Numerical apertur	0.5 for fiber length > 2 m
Refractive index	2.2
Attenuation at 10 μm	<0.1 dB/m
at 5 μm	<0.3 dB/m
Maximum length	10 m
Inner cover	Loose polymer tube
Outer cover	PEEK tube

the fingerprint region of infrared spectra for the characterization of edible oils has recently been emphasized by Gillen and Cabo.[16] The composition of olive oil samples mixed with edible seed oils at different concentrations was studied by the same authors, who recorded mid-infrared transmission spectra of several blends.[17] A comparison of methods using mid-infrared and Raman spectra for the authentication of edible oils was presented recently by Marigheto et al.[18] Another issue with respect to olive oil composition analysis is the determination of lipid oxidation in edible oils, which has been tackled by near-infrared spectroscopy.[19] Alternatively, the oxidative deterioration of edible oils by heating has been intensively analyzed by the group of Moya Moreno et al. by using Fourier transform infrared (FT-IR) spectroscopy; see for example Ref. 20. Other important key components in olive oil are free fatty acids, which have been quantified by straightforward ATR spectroscopy, using PLS calibration models based on specific mid-infrared wavenumber intervals.[21]

The analytical challenge here is the quantification of sunflower oil in extra virgin olive oil samples by mid-infrared ATR spectroscopy using a fiber-optic probe, which needs high-quality spectroscopy, in particular high spectral reproducibility and large signal-to-noise ratios. The set of olive oil samples used here was unique, because it had been collected from many different areas within Greece, so that for the first time the regional variance in composition could be taken into account for adulterant assay development and robustness testing. Multivariate calibration with partial least-squares, based on spectral intervals in the mid-infrared spectral range with and without additional wavelength selection, was considered. The selection procedure generally led to improved performance and robustness of the calibration models. Results obtained here are compared with those of a previous study for which Fourier transform Raman spectroscopy was applied.[22]

EXPERIMENTAL

Infrared spectra were recorded on an FT-IR spectrometer (Model Vector 22; Bruker Optik GmbH, Karlsruhe, Germany), equipped with a flexible silver halide optical fiber probe for remote ATR spectroscopy. The infrared beam exiting the FT-IR spectrometer was coupled into the silver halide fiber by an off-axis parabolic mirror with a numerical aperture of 0.6. The characteristics of the silver halide optical fiber, supplied by infrared fiber sensors (Aachen, Germany), are presented in Table I.

The silver halide fiber-optic probe had a shaft containing one fiber for transmitting and one fiber for receiving

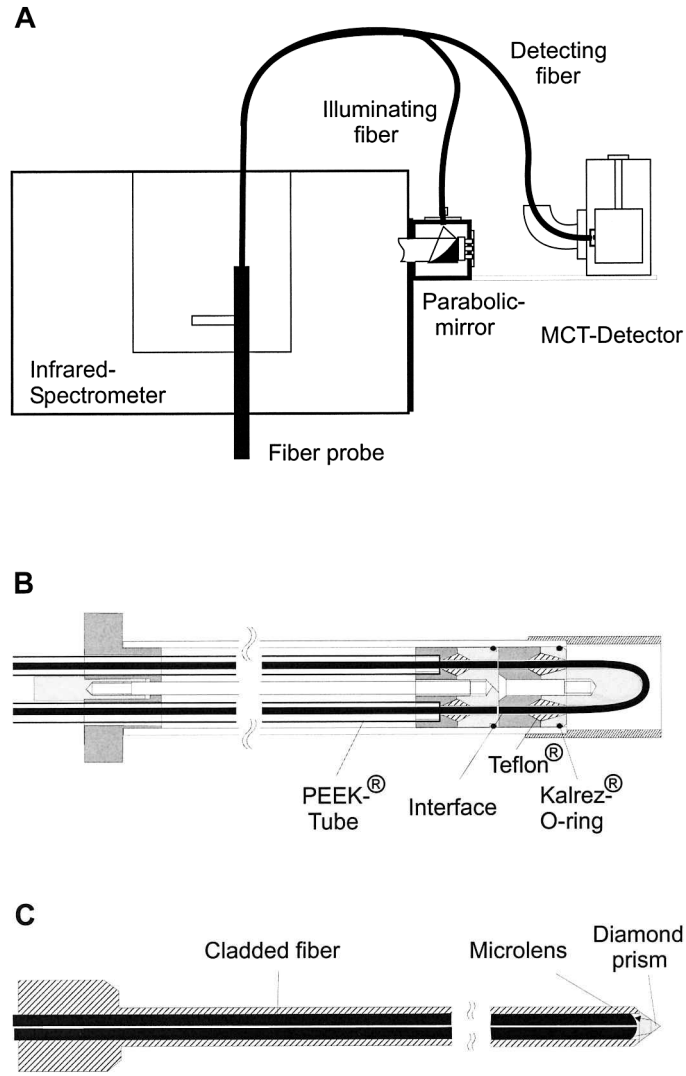

FIG. 1. Experiment setup with FT-IR spectrometer and fiber probe coupling to spectrometer and external MCT detector.

infrared energy from the ATR measuring head. The transmitting and receiving fibers were 2 m in length with a diameter of 750 μm and a numerical aperture of 0.5. The shaft length was 20 cm (12 mm in diameter) and had means for attaching exchangeable short U-turned silver halide fiber sections for ATR measurements (for the experimental setup, see Fig. 1). The sensitivity of the ATR element depends on the length and the bending radius of the silver halide fiber, which is in contact with the sample medium. The maximum sensitivity is reached at the lower end of the bent fiber piece and can easily be increased by reducing the bending radius down to values smaller than the diameter of the fiber. In the experiments presented in this paper, a fiber ATR element with a bending radius of 4 mm was used. The receiving fiber was directly coupled to a liquid nitrogen-cooled semiconductive mercury-cadmium-telluride detector (MCT) with the use of a microlens at the fiber end facing the detector element (Infrared Associates, Inc., Stewart, FL). The signal was amplified by a preamplifier, which was matched to the detector to ensure low noise.

A second fiber-coupled probe with a diamond ATR sensor element was developed. The probe allows two in-

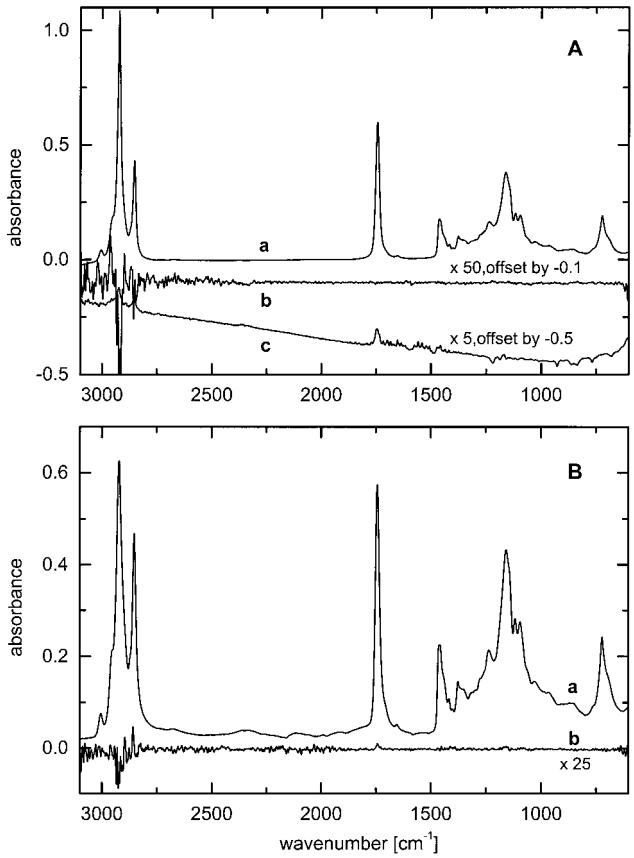

FIG. 2. (**A**) Absorbance spectrum of an olive oil sample measured by the silver halide fiber probe (***a***), absorbance noise from two consecutive single-beam spectra with olive oil sample (128 scans, 4 cm^{-1} spectral resolution) (***b***), and degradation of fiber sensor transmission after measurement of 100 olive oil spectra (***c***). (**B**) Absorbance spectrum of an olive oil sample measured by the fiber coupled diamond probe (***a***); absorbance noise under same conditions as given above (***b***).

ternal reflections in the diamond prism, which was immersed in the sample to be measured. Following the IR radiation attenuation by the sample, a second fiber led the infrared radiation to the detector as described above (see Fig. 1C).

The spectroscopic performance of both the silver halide fiber-optic probe and the fiber-coupled diamond probe concerning absorption band intensities and spectral noise is presented in Fig. 2. All absorbance spectra were recorded with a measuring time of 1 min for 128 coadded scans and a spectral resolution of 4 cm^{-1}. In the long wavelength region, the spectral response was limited by the cutoff of the MCT detector at 580 cm^{-1}, whereas for the short wavelength region, scattering losses of the silver halide fibers reduced the signal-to-noise ratio significantly. Because of the low single-beam intensities around 3000 cm^{-1}, the photometric accuracy reached with the fiber-optic probe was degraded compared to that of the diamond probe, so that the absorption band intensities in that region differ significantly from each other.

Measurements were obtained for all 88 samples in a set covering one year's harvest from different Mediterranean sites (22 pure olive oil samples and 66 spiked samples containing 2, 5, and 10% by weight of sunflower oil, respectively). The samples were stored in the dark at room temperature. After measurements using the fiber probe, a time lapse of 3½ months occurred before the sample set was measured again with the diamond probe. One turbid sample contained a significant amount of water and was discarded from the calibrations.

Absorbance spectra from 3000 to 600 cm^{-1} were collected with the shaft of the silver halide fiber-optic probe fixed in a mechanical holder and dipped into the olive oil sample to be studied. The probe was cleaned with ethanol between samples. A background measurement with the fiber probe was recorded after each sample measurement to ensure that sample contamination by the previous sample was completely avoided. Any degradation of the fiber transmission could be detected by inspecting the ratio of corresponding spectra of the cleaned sensor tip. An example is provided with Fig. 2A for measurements at the end and the beginning of the measurement campaign, illustrating the attenuation within the sensing fiber piece after the measurement of about 100 samples of olive oil. Background measurements for the diamond sensor tip were recorded every eight samples to compensate for any possible drift—e.g., changes in temperature of the source or in the spectrometer atmosphere. The diamond tip and the lower casing of the probe, which came into contact with the sample, were cleaned after every measurement with ethanol and dried by pressurized nitrogen gas. During the measurements the spectrometer was continuously purged by dry nitrogen.

Multivariate calibration using absorbance spectra was carried out by using the partial least-squares PC-software package from CAMO, ASA, Oslo, Norway (the Unscrambler) and a second package programmed in MATLAB (The Mathworks, South Natick, MA) by the authors. Apart from full spectrum interval regression, a special wavelength selection procedure was chosen, which rendered improved and more robust models for statistical calibrations. The selection was done stepwise by using pairs of selected individual wavelengths, as suggested by the decreasing weights of the minima and maxima of the optimum PLS regression vector, calculated from all sampling points within a broad spectral interval provided by *a priori* knowledge of sunflower oil absorption bands; for further details, see Ref. 23.

With ill-conditioned linear equation systems, such as found in analytical spectroscopy with the use of rather similar samples for calibration, the validation of calibration models (i.e., testing their prediction performance) is of utmost importance. For such calibrations, the standard error of calibration (SEC) is not an appropriate statistic,[24] although with well-conditioned, largely overdetermined linear equation systems, the differences between SEC and corresponding results obtained from testing with calibration-independent samples decrease. The calibration data are usually split into calibration and validation subsets, which is a reasonable strategy when a large number of standards are available or the composition complexity of the calibration samples is low. An appropriate spectral quality (i.e., high signal-to-noise ratio, good baseline stability, adequate photometric accuracy, and absence of signal nonlinearities) is essential. With a limited number of standards under more adverse conditions, cross-validation with ''leave-one-out'' strategy is frequently used. Here, one standard is removed from the calibration set, a regression is calculated, and the concentration is predicted

by using the calibration model for that single standard. These steps are repeated, until all standards are considered. The root mean squared error of prediction [RMSEP = $(\Sigma\ (c_{\mathrm{ref},i} - c_{\mathrm{pred},i})^2/M)^{1/2}$ with M samples, or standard error of prediction (SEP)] is a suitable statistic for determining the optimum calibration model with stepwise increased number of PLS factors. In order to study the robustness of our calibration models, leave-ten-out cross-validation was also applied after an additional sample order randomization within the whole calibration sample population. SEP results are reported for the calibration models with spectral variable selection.

All spectra files were initially imported from the JCAMP-DX format[25] into the Unscrambler multivariate analysis program. For our own calibration MATLAB package, all spectra and calibration data were transferred to a personal computer for further data processing using the MATLAB binary export format of the Unscrambler package.

RESULTS AND DISCUSSION

The spectra of pure sunflower and olive oil samples show only slight spectral differences, which can be attributed to the differences in composition (the glycerolesters of the following fatty acids are found on average in sunflower oil: 66.2% linoleic acid, 25.1% oleic acid, 5.6% palmitic acid, 2.2% stearic acid, 0.9% arachic acid; mean composition of olive oil: 66.3% oleic acid, 12.3% linoleic acid, 8.9% palmitic acid, 4.9% eicosanic acid, 4.7% palmitoleic acid, 2.4% stearic acid, 0.8% behenic acid, 0.6% linolenic acid, 0.3% arachic, 0.2% myristic acid; oleic acid as the main constituent can amount up to 85%).[26] Example spectra are shown in Fig. 3A, whereas in Fig. 3B the spectra resulting from the addition of 2, 5, and 10% sunflower oil, to a native olive oil sample, are shown. The difference spectra were obtained with the silver halide fiber probe. These slight differences become even harder to observe when the geographical variance in composition further complicates the picture.

Differences in the spectra recorded by using the silver halide fiber and diamond probe are evident in Fig. 2. This is because of the different geometry of the probes, their different refractive indices, and the strong absorptions within the diamond material. This contrast gives rise to some additional absorption bands within the spectral region of 2700 to 1800 cm^{-1}. The differences for the population mean spectra are shown in Fig. 4A, where it is seen that, as well as intensity differences, there is also a slight wavenumber shift for the 1750 cm^{-1} absorption band between the two probes, which has its origin in the dissimilar refractive indices of the different ATR crystals employed. Various statistical figures for the two populations of spectra are provided in Figs. 4B and 4C. The lowest traces refer to the so-called property correlation spectrum **s**, which is calculated by using the concentration values of sunflower oil in the samples measured:

$$\mathbf{s} = c_{\mathrm{av}}\mathbf{A}_{\mathrm{mc}}\mathbf{c}_{\mathrm{mc}}/[\mathbf{c}_{\mathrm{mc}}^{\mathrm{T}}\mathbf{c}_{\mathrm{mc}}]$$

where $\mathbf{c}_{\mathrm{mc}}$ is the vector of mean-centered sunflower oil concentration values, c_{av} is the mean value, and $\mathbf{A}_{\mathrm{mc}}$ is the matrix of mean-centered sample spectra. The resulting spectrum is proportional to the first loading vector of

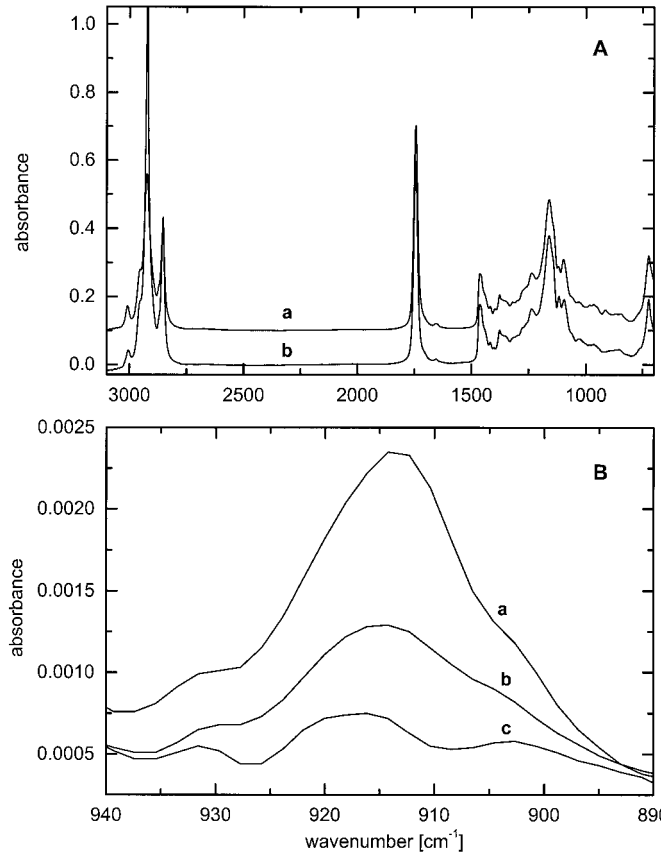

FIG. 3. (**A**) Absorbance spectra of sunflower oil (***a***) and of an olive oil sample (***b***); (**B**) difference spectra of olive oil samples contaminated by sunflower oil with a concentration of 10% (***a***), 5% (***b***), and 2% (***c***), respectively (the spectra were obtained by scaled absorbance subtraction using the pure olive oil spectrum).

the PLS matrix decomposition, which is usually normalized to unit length; see for example Ref. 27. Under the condition that other components are uncorrelated to the sunflower oil concentration, an all-positive spectrum is obtained, representing the absorbance spectrum of the spiked compound at the population mean concentration. For both probes, a very similar property correlation spectrum is obtained.

Differences are, however, evident for the standard deviation spectrum of the populations measured. Inspection of the standard deviation for the C=O stretch vibration band reveals that the standard deviation is a factor of 3 larger than that of the corresponding ''spectrum'', calculated from the spectral population recorded with the use of the diamond probe. The shape of the standard deviation spectrum obtained with the silver halide probe resembles that of the oil spectra, which underlines that most of the spectral variance is due to overall intensity changes, whereas the reproducibility of spectral measurement is much higher with the diamond probe. Therefore, the variation because of sunflower additions becomes the dominating factor. The similarity of the standard deviation spectrum and that of the property correlation spectrum, derived from spectra obtained with the diamond probe, is remarkable. We calculated another statistical figure, $\sigma^2_{\mathrm{dif}} = \sigma^2_{\mathrm{total}} - \sigma^2_{\mathrm{pure}}$, where $\sigma^2_{\mathrm{total}}$ is the variance calculated from all sample spectra measured by the individual probes, and σ^2_{pure} is the spectral variance calculated

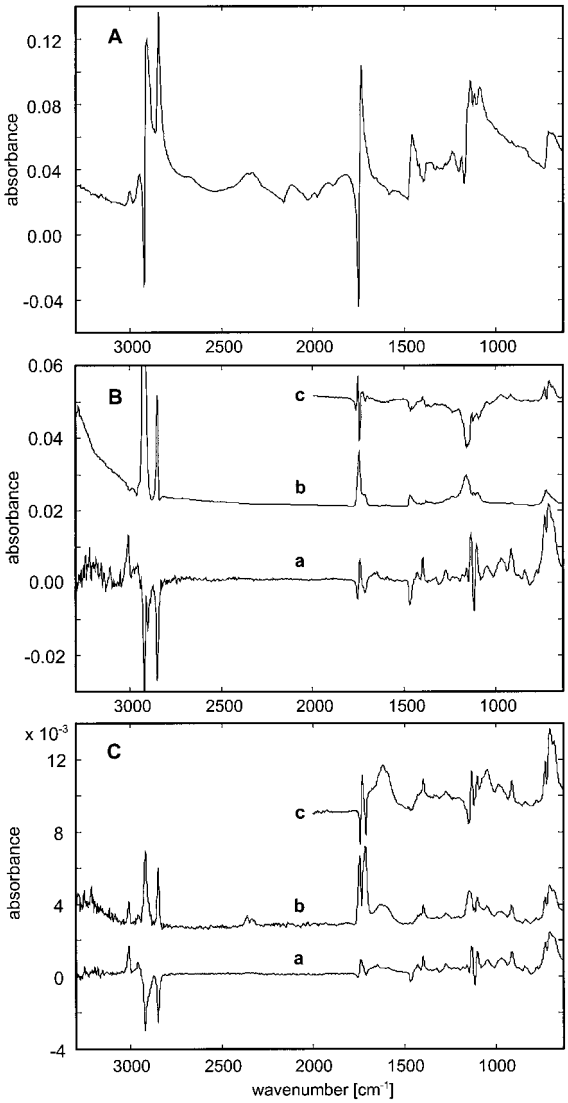

FIG. 4. (**A**) Difference spectrum of the mean population spectrum of pure and contaminated olive oil samples as measured by the diamond probe minus that as measured by the silver halide fiber probe. (**B**) Property correlation spectrum using the sunflower oil concentrations (***a***), standard deviation spectrum of the population spectra (***b***), and difference of the spectral variances as calculated from all samples minus variance of the pure olive oil samples (***c***). Spectra were obtained with the silver halide fiber probe. (**C**) as for part **B**, but spectra were measured by the fiber-coupled diamond probe.

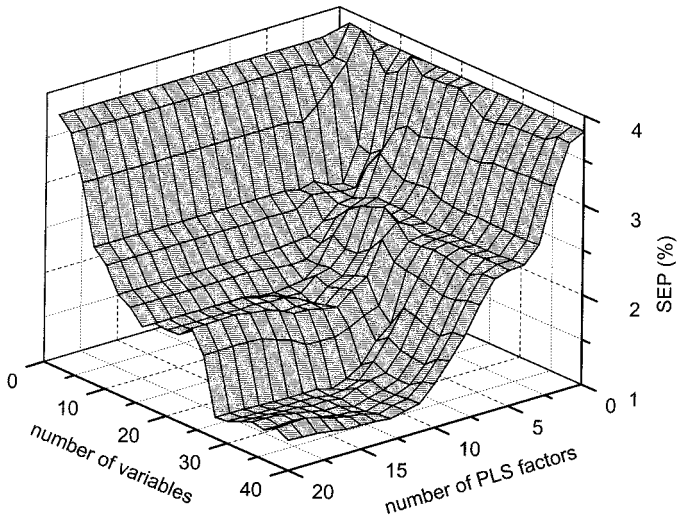

FIG. 5. Standard error of prediction for PLS calibration models derived for the sample population measured by the silver halide fiber probe in dependence of the number of selected spectral variables and the number of PLS factors used for calibration model calculation.

for the pure olive oil samples only. The variance difference, calculated for the silver halide probe, highlights spectral features which are clearly related to the sunflower oil additions (see Fig. 4B, upper trace).

A selection of spectral intervals was tested for multivariate calibration based on partial least-squares. Results of these calculations are summarized in Table II. Best results for standard errors of prediction, obtained from cross-validation, were around 1.8%, when data from broad spectral intervals were employed. The number of wavelengths required for optimal spectroscopic calibration is still a subject of intense debate. Several investigations have been reported, where results were compared from full-spectrum PLS calibration with those improved values from multiple linear regression (MLR); for the latter, usually a reduced number of spectral variables is selected for spectral calibration. With our selection strategy, significantly improved results were obtained. In Fig. 5, the standard error of prediction is plotted vs. the number of spectral variables, and a third axis provides the dependency on the number of PLS factors used for the respective individual calibrations. The global minimum under these conditions is found for 28 spectral variables and a PLS rank of 12 (SEP = 1.2%). The spectra recorded by means of the diamond probe were slightly more noisy compared to the other probe used, so that the optimum

TABLE II. PLS calibration results for predicting sunflower seed oil concentration in different olive oil samples. The SEP values were obtained by leave-one-out cross-validation (exemplary results from leave-ten-out cross-validation are listed in parentheses).

Probe type	Spectral range (cm^{-1})	Number of variables	PLS rank	SEP (%)
Fiber	3060–2730, 1790–1630, 1500–630	705	7	2.6
Fiber	1790–1630, 1500–630[a]	534	14	1.7
Fiber	1500–630	451	12	1.8
Fiber	Spectral variable selection[a]	28	12	1.2 (1.2)
Diamond	3060–2730, 1790–1630, 1500–630[b]	1411	12	1.8
Diamond	1500–630	902	15	1.9
Diamond	1500–630 (without two outliers)	902	16	1.7_5
Diamond	Spectral variable selection[b]	26	7	1.5 (1.5)
Diamond	Spectral variable selection[b]	36	17	1.4

[a,b] The spectral variable selection was based on the spectral intervals that led to optimum calibration results.

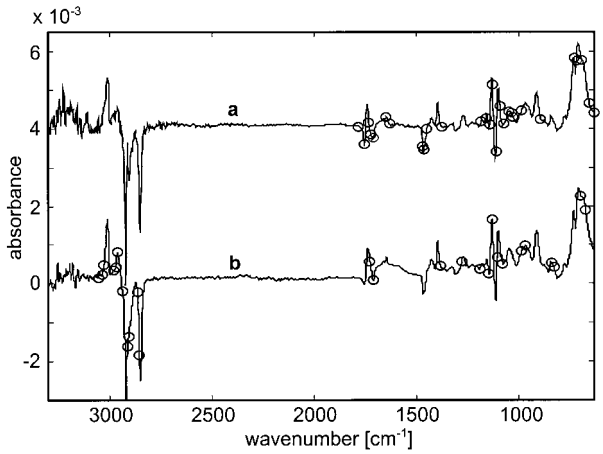

FIG. 6. Illustration of spectral variables selected under the scheme of choosing extreme values of an optimum regression vector which was calculated from a broad spectral interval evaluation. The variables are indicated by open circles within the property correlation spectra which were obtained from the ATR spectra recorded from pure and adulterated olive oil sample and corresponding sunflower oil concentrations, using the silver halide fiber probe (***a***) and the fiber-coupled diamond probe (***b***), respectively.

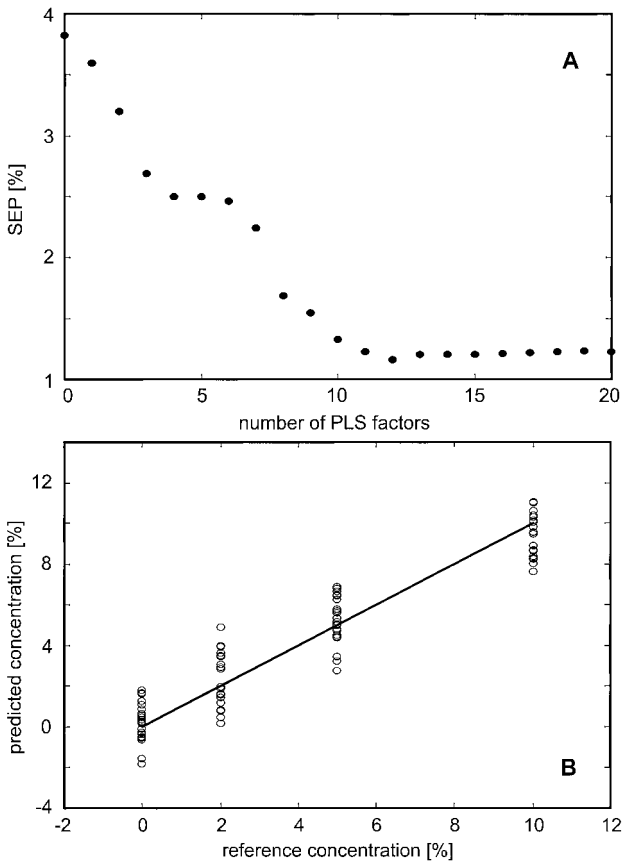

FIG. 7. Calibration results for sunflower oil concentrations added to olive oil samples (spectra were obtained with the silver halide fiber ATR probe). (**A**) Standard error of prediction from leave-one-out cross-validation for PLS calibration models based on 28 selected spectral variables from the spectral interval of 1790–630 cm^{-1} vs. number of PLS factors. (**B**) Scatter plot of PLS predicted sunflower oil concentrations versus values obtained by weight (the straight line is the ideal calibration function).

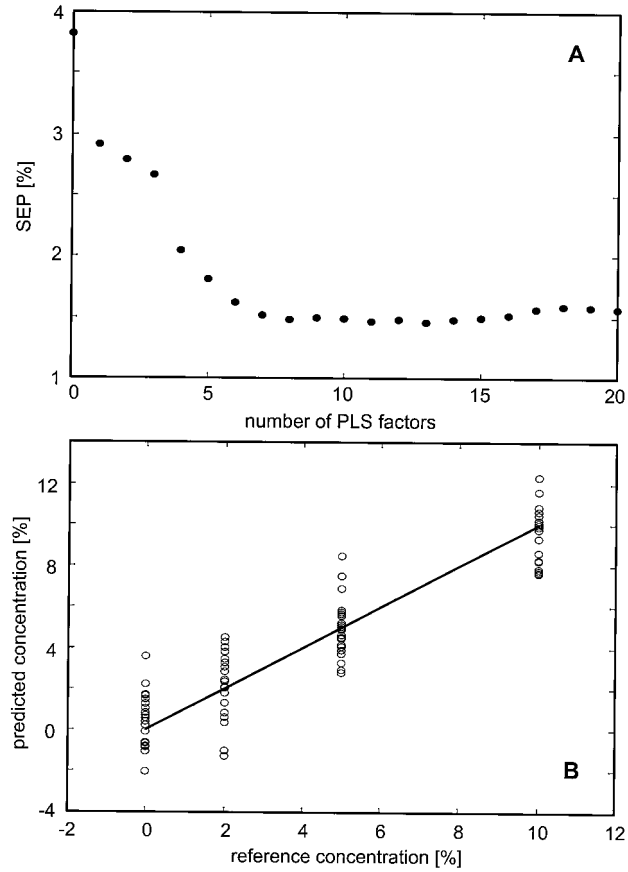

FIG. 8. Calibration results for sunflower oil concentrations added to olive oil samples (spectra were obtained with the fiber-coupled diamond ATR probe). (**A**) Standard error of prediction from leave-one-out cross-validation for PLS-calibration models based on 26 selected spectral variables from the spectral interval of 3060–630 cm^{-1} vs. number of PLS factors. (**B**) Scatter plot of PLS predicted sunflower oil concentrations vs. values obtained by weight (the straight line is the ideal calibration function).

standard error of prediction, found for 36 spectral variables and a PLS rank of 17, was 1.4%.

Detailed calibration results for the cases comprising a selection of less than 30 spectral variables are presented below. The specific spectral wavenumbers chosen for optimized prediction are elucidated in Fig. 6, which are based on the spectral data recorded by means of the two sensor probes employed. A presentation within the corresponding property correlation spectra is used, which also represent the scaled PLS regression vectors based on the respective first PLS factors. This regression vector is shaped by further implementing PLS factors to improve the prediction performance of the calibration models. For the calibration models that were based on a reduced number of spectral variables, well-conditioned linear equation systems resulted with SEP values which change only insignificantly after the optimum calibration matrix rank has been reached. The least-squares solution is obtained by the inversion of the full-rank calibration matrix. The corresponding Figs. 7A and 8A illustrate the PLS rank dependency of the SEP values under the constraint of 28 and 26 spectral variables selected, whereas Figs. 7B and 8B provide the scatter plots for the optimum PLS calibration models using leave-one-out cross-validation. Nearly identical SEP values were obtained when a cross-

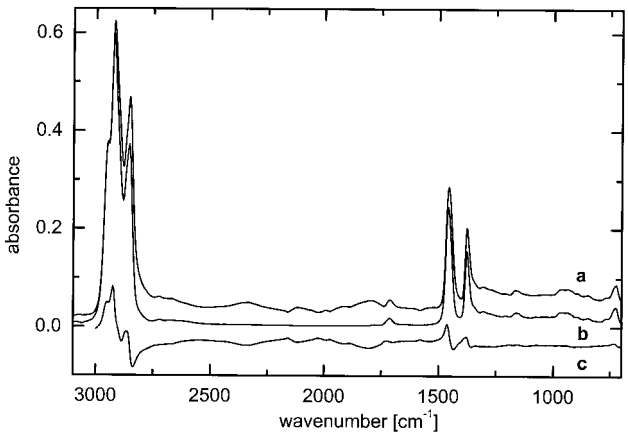

FIG. 9. ATR spectra of Nujol obtained with the fiber-coupled diamond probe (***a***) and that recorded using the silver halide fiber probe (***b***); also shown in ***c*** is the difference spectrum of traces ***b*** minus ***a***.

validation strategy under leave-ten-out was applied. The regional variation in olive oil composition gives rise to the broad scatter in the ordinate values, which cannot be overcome with the IR calibration methodology. We also tested the prediction performance under the scheme whereby, successively, samples from two regions were deleted simultaneously from the calibration sample set, using leave-eight-out cross-validation. The SEP value for the fiber-coupled diamond sensor, for example, was the same with an eight PLS factors model, when compared to the result calculated with leave-one-out cross-validation.

When we compare our previous PLS calibrations (without wavelength selection) based on Fourier transform Raman spectra of these pure and adulterated olive oil samples with the results obtained in this study, we note a marked improvement with these techniques: There is a significant reduction in the prediction error by a factor of 2.5 compared to the evaluation of corresponding FT-Raman data. However, the ATR measurement technique requires that the sample be brought into contact with the sensing probe, whereas the FT-Raman technique allows for a spectrum measurement through the glass container.

The diamond-based probe is often recommended for ATR measurements, in particular when chemical inertness is required or high pressure must be applied to achieve good contact of the sample with the ATR crystal, but spectral artifacts connected to such a measurement are seldom discussed. Another example is provided here with Nujol spectra, which were recorded with both probes (see Fig. 9). The mid-infrared spectrum of this compound possesses broad spectral intervals free of absorption bands. For highlighting the artifacts, the difference spectrum is shown, which also again illustrates slight wavenumber shifts in the positions of strong absorption bands under the ATR measurement conditions inherent for both sensor types.

CONCLUSION

The fiber-based ATR probes proved to be powerful tools for determining the concentrations of olive oil samples contaminated by sunflower oil additions. Contributions greater than 2% by weight could be quantified without ambiguity with the silver halide fiber probe. There is a slight deterioration in the spectral performance, which does not perturb the analysis over a long time interval, as long as proper background spectra are recorded for calculating the absorbance spectra. Another advantage is that, after probe degradation, the probe can be replaced without problems. This design also allows different types of probes to be optimized for sample attenuation of the IR radiation. The performance of the diamond probe is slightly lower with respect to random noise features, which can be overcome, within the transparent spectral regions, by accumulating more interferograms. The remote sensing capability is another positive feature, which is similar to that for fiber probes used in the near-infrared spectral range that are based on quartz fibers. Such devices have been mostly employed, with the use of diffuse reflectance for powders or transmission spectroscopy for fluids, for the identification of raw materials on receipt (e.g., in the pharmaceutical industry), as well as for verification of the composition of pharmaceutical formulations before the final products leave the plant premises. Similar powerful probes can be constructed with silver halide fibers, employing the ATR measurement technique for liquids, as well as for powders.

ACKNOWLEDGMENTS

The authors from ISAS acknowledge gratefully the financial support by the Ministerium für Schule, Wissenschaft und Forschung des Landes Nordrhein-Westfalen and the Bundesministerium für Bildung und Forschung. The European Union is to be thanked for some funding for this work (EU Contract No. AIR2-CT 92-1224).

1. L. Dolmatova, C. Ruckebusch, N. Dupuy, J.-P. Huvenne, and P. Legrand, Appl. Spectrosc. **52,** 329 (1998).
2. H. M. Heise, "Clinical Applications of Near- and Mid-Infrared Spectroscopy", in *Infrared and Raman Spectroscopy of Biological Materials,* H.-U. Gremlich and B. Yan, Eds. (Marcel Dekker, New York, 2001), Chap. 8, p. 259.
3. W. M. Doyle, Process Control Qual. **2,** 11 (1992).
4. D. Picque, D. Lefier, R. Grappin, and G. Corrieu, Anal. Chim. Acta **279,** 67 (1993).
5. F. Cadet, C. Robert, and B. Offmann, Appl. Spectrosc. **51,** 369 (1997).
6. Y. Gotshal, I. Adam, and A. Katzir, Proc. SPIE-Int. Soc. Opt. Eng. **3262,** 192 (1998).
7. A. Brooks, N. I. Afanasyeva, V. Makhine, R. F. Bruch, and B. McGregor, Proc. SPIE-Int. Soc. Opt. Eng. **3596,** 140 (1999).
8. H. M. Heise, A. Bittner, L. Küpper, and L. N. Butvina, J. Mol. Structure **410/411,** 521 (1997).
9. H. M. Heise, L. Küpper, and L. N. Butvina, Sensors Actuators B **51,** 84 (1998).
10. L. Webster, P. Simpson, A. M. Shanks, and C. F. Moffat, Analyst **125,** 97 (2000).
11. J. P. Favier, D. Bicanic, J. Cozijnsen, B. Van Veldhuizen, and P. Halander, J. Am. Oil Chem. Soc. **75,** 359 (1998).
12. I. J. Wesley, F. Pacheco, and A. E. J. McGill, J. Am. Oil Chem. Soc. **73,** 515 (1996).
13. Y. W. Lai, E. K. Kemsley, and R. H. Wilson, Food Chem. **53,** 95 (1995).
14. N. Dupuy, L. Duponchel, J. P. Huvenne, B. Sombret, and P. Legrand, Food Chem. **57,** 245 (1996).
15. D. B. Dahlberg, S. M. Lee, S. J. Seth, and J. A. Vargo, Appl. Spectrosc. **51,** 1118 (1997).
16. M. D. Guillen and N. Cabo, J. Agric. Food Chem. **46,** 1788 (1998).

17. M. D. Guillen and N. Cabo, Fett/Lipid **101,** 71 (1999).
18. N. A. Marigheto, E. K. Kemsley, M. Defernez, and R. H. Wilson, J. Am. Oil Chem. Soc. **75,** 987 (1998).
19. H. Takamura, N. Hyakumoto, N. Endo, T. Matoba, and T. Nishiike, J. Near Infrared Spectrosc. **3,** 219 (1995).
20. M. C. M. Moya Moreno, D. Mendoza Olivares, F. J. Amezquita Lopez, J. V. Gimeno Adelantado, and F. Bosch Reig, Talanta **50,** 269 (1999).
21. E. Bertran, M. Blanco, J. Coello, H. Iturriaga, S. Maspoch, and I. Montoliu, J. Am. Oil Chem. Soc. **76,** 611 (1999).
22. A. N. Davies, P. McIntyre, and E. Morgan, Appl. Spectrosc. **54,** 1864 (2000).
23. H. M. Heise and A. Bittner, Fresenius' J. Anal. Chem. **359,** 93 (1997).
24. R. Marbach and H. M. Heise, Trends Anal. Chem. **11,** 270 (1992).
25. R. S. McDonald and P. A. Wilks, Jr., Appl. Spectrosc. **42,** 151 (1988).
26. *Römpps Chemie-Lexikon,* O.-A.Neumüller, Ed. (Franckh'sche Verlagshandlung, Stuttgart, 1985), 8th ed.
27. H. M. Heise, R. Marbach, G. Janatsch, and J. D. Kruse-Jarres, Anal. Chem. **61,** 2009 (1989).